Continuum shell model

Alexander Volya[1] and Vladimir Zelevinsky[2]
[1]*Department of Physics, Florida State University, Tallahassee, Florida 32306-4350, USA*
[2]*NSCL and Department of Physics and Astronomy, Michigan State University, East Lansing, Michigan 48824-1321, USA*
(Received 20 September 2005; revised manuscript received 12 October 2006; published 22 December 2006)

The continuum shell model is an old but recently revived method that traverses the boundary between nuclear many-body structure and nuclear reactions. The method is based on the non-Hermitian energy-dependent effective Hamiltonian. The formalism, interpretation of solutions, and practical implementation of calculations are discussed in detail. The results of the traditional shell model are fully reproduced for bound states; resonance parameters and cross-section calculations are presented for decaying states. Particular attention is given to one- and two-nucleon reaction channels, including sequential and direct two-body decay modes. New calculations of reaction cross sections and comparisons with experimental data for helium and oxygen isotope chains are presented.

DOI: 10.1103/PhysRevC.74.064314 PACS number(s): 21.60.Cs, 24.10.Cn, 27.20.+n

I. INTRODUCTION

New horizons are in sight in the field of nuclear physics as we move away from the line of nuclear stability. In everyday experience we observe only a tiny fraction of the nuclear world, but recent advances in observational techniques reveal a hidden realm of extraordinary nuclear complexes. The term "exotic" is commonly used to highlight the unusual nature of newly discovered nuclear systems where structure and stability are governed by the intricate interplay of quantum many-body physics and the dynamics of nuclear reactions. Weakly bound nuclei and unstable resonances appear as important links in the chain of nuclear evolution. In the cosmos, their structure and properties are central for energy generation in stars and production of elements in the universe. Furthermore, quantum objects of mesoscopic nature are common to many fields of science, including but not limited to atoms and molecules, nanoscale condensed matter systems, atomic clusters, atoms in traps, and prototypes of quantum computers [1]. In many applications to mesoscopic systems one needs to understand and utilize the features of marginal stability and the strong coupling between the discrete spectrum and the continuum.

The mean field along with the corresponding shell structure is a starting point in the theoretical analysis of a quantum many-body system. The shell structure itself becomes exotic on the borderline of the continuum [2–5]. Single-particle, pairwise, and cluster excursions into the continuum become essential, forming halo states and resulting in complex mixing of internal many-body states and continuum configurations. The problems of the continuum shell model (CSM), or combining the description of reactions with the structure calculations, have been discussed almost since the dawn of the shell model, and these are summarized in the classical text [6]. However, fueled by the discoveries of exotic systems, the acute need in theoretical understanding, and growing computational capabilities, this subject has recently received due attention, leading to significant advances during the past few years. In this work we concentrate on the version of the CSM [7,8] that goes back to the Feshbach projection formalism [9–12] and, even much earlier, to the approach by Weisskopf and Wigner [13] and works in atomic physics by Rice [14] and Fano [15,16]. Alternative formulations, such as those of Refs. [17–20] (see the review in Ref. [21]), were also successfully developed recently.

The specific attractive features of the approach discussed in the following are the natural unification of structure and reactions, full agreement with the results of the traditional shell model (SM) in the discrete spectrum, correct energy behavior of resonance widths and reaction cross sections near thresholds, self-consistent consideration of isotope chains, and exact unitarity of the scattering matrix. At this point we use the standard residual interactions adjusted in numerous applications of the conventional SM, although the problem of better interactions in the continuum remains open (with the first steps in this direction being made in Ref. [22]).

We organize the discussion here starting with the formal description of the CSM approach in the following section; this will be the formalism that we imply under the term CSM throughout this work. In Sec. II we also discuss mathematical details of the formulation, relation to observables, and the unitarity of the scattering matrix. Section III is devoted to the detailed consideration of different parts of the approach; we consider the limit of the conventional SM, one-body decay channels, and sequential and direct two-body channels. The realistic applications are shown and compared with experiment in Sec. IV.

II. FORMULATION OF THE CONTINUUM SHELL MODEL

A. Effective Hamiltonian

In what follows we assume that the many-body Hilbert space is spanned by Slater determinants constructed from the single-particle (s.p.) orbitals $|j\rangle$ in the mean field. Using the notation of secondary quantization we denote the s.p. creation and annihilation operators for discrete orbitals as $b_j^\dagger$ and b_j, labeled by a combined discrete label j. For the continuum states we use s.p. operators $b_j^\dagger(\epsilon)$ and $b_j(\epsilon)$, which are labeled with the discrete index j and the continuous s.p. energy

variable ϵ. If properly constructed for a mean-field potential (see the later discussion related to one-body reactions), these states are automatically orthogonal and form a complete set. In this work, however, we require only separate orthogonality of the bound states, $[b_j, b^\dagger_{j'}]_+ = \delta_{jj'}$, and of the continuum states normalized according to $[b_j(\epsilon), b^\dagger_{j'}(\epsilon')]_+ = \delta(\epsilon - \epsilon')\,\delta_{jj'}$.

The full many-body space can be separated into two parts. The set of N-particle bound states $|1; N\rangle = b^\dagger_{j_1} \dots b^\dagger_{j_N}|0\rangle$ form the "internal" space, $\mathcal{P}$, where the index $1 = \{j_1, j_2, \dots, j_N\}$ labels the Slater determinant, the m-scheme representation in the SM terminology. The remaining space, $\mathcal{Q}$, is the "external" continuum, that is, many-body states that contain one or more particles in the continuum. The external many-body states $|c, E\rangle$ are labeled by total continuum energy E and the set of asymptotic variables c that define a reaction channel (including the characteristics of the residual nucleus). The channel variable c is discrete only in the case of the one-body decay where energy conservation fully determines energies of the two decay products. In general this variable is continuous, containing relative energies or momenta of decay products needed for full specification of the final state. In the description of the formalism that follows we use the notation $\sum_c$ and $\delta_{cc'}$, which in the case of the continuous channel variables should be interpreted as $\int dc$ and $\delta(c - c')$, respectively. In Sec. III D, where channel c in the two-body decay implies the presence of the relative energy variable, the sum over channels is explicitly given in terms of an integral. By construction, the many-body states in $\mathcal{P}$ and $\mathcal{Q}$ spaces are mutually orthogonal and normalized as

$$\langle 1|2\rangle = \delta_{12}, \quad \langle c; E|c'; E'\rangle = \delta_{cc'}\delta(E - E'). \tag{1}$$

Within the total space $\mathcal{P} + \mathcal{Q}$, we solve the stationary Schrödinger equation

$$H|\alpha; E\rangle = E|\alpha; E\rangle, \tag{2}$$

where the full wave function $|\alpha; E\rangle$ is in general a superposition of internal states $|1\rangle$ and external states $|c; E'\rangle$,

$$|\alpha; E\rangle = \sum_1 \alpha_1(E)|1\rangle + \sum_c \int dE' \alpha_c(E'; E)|c; E'\rangle. \tag{3}$$

The Hamiltonian H has parts acting within and across $\mathcal{P}$ and $\mathcal{Q}$ spaces,

$$H = H_{\mathcal{P}\mathcal{P}} + H_{\mathcal{P}\mathcal{Q}} + H_{\mathcal{Q}\mathcal{P}} + H_{\mathcal{Q}\mathcal{Q}}. \tag{4}$$

The external states can be eliminated by introducing a propagator that acts exclusively within $\mathcal{Q}$ space,

$$G_{\mathcal{Q}\mathcal{Q}}(E) = \frac{1}{E - H_{\mathcal{Q}\mathcal{Q}} + i0}, \tag{5}$$

where the infinitesimal imaginary displacement selects the appropriate boundary conditions for the scattering problem. Next we assume that the channel labels c correspond to the eigenchannels [23] in the $\mathcal{Q}$ space, $H_{\mathcal{Q}\mathcal{Q}}|c; E\rangle = E|c; E\rangle$. Then the Schrödinger equation (2) "projected" into the subspace P becomes

$$\sum_2 \Bigg[\langle 1|H|2\rangle + \sum_c \int dE' \times \frac{\langle 1|H - E|c; E'\rangle\langle c; E'|H - E|2\rangle}{E - E' + i0} - \delta_{12}E\Bigg]\alpha_2 = 0. \tag{6}$$

The amplitude of the continuum admixture in the full wave function (3) is

$$\alpha_c(E'; E) = \frac{\sum_1 \alpha_1(E) A_1^{c*}(E', E)}{E - E' + i0}, \tag{7}$$

where we introduced the following notation for the $H_{\mathcal{P}\mathcal{Q}}$ coupling amplitude:

$$A_1^c(E', E) = \langle 1|H - E|c; E'\rangle. \tag{8}$$

This amplitude depends on the continuum variable of energy E' and running energy E. As follows from the definition (8), there is no explicit E dependence when internal and external spaces are orthogonal. However, the important E' dependence remains; the kinematic factors included in the definition of the channel states $|c; E'\rangle$ ensure that the phase space shrinks to zero and the channel c becomes closed below threshold energy E_c characteristic for a given channel. Whence, the amplitudes A_1^c vanish at $E' < E_c$.

The set of equations (6) for coefficients α_1 looks like an eigenvalue problem with the effective Hamiltonian matrix $\mathcal{H}$ in the intrinsic space defined as

$$\langle 1|\mathcal{H}(E)|2\rangle = \langle 1|H|2\rangle + \sum_c \int dE' \frac{A_1^c(E', E) A_2^{c*}(E', E)}{E - E' + i0}. \tag{9}$$

The integral in Eq. (9) can be further decomposed into its Hermitian part (principal value), $\Delta(E)$, and the anti-Hermitian part, $-(i/2)W(E)$,

$$\sum_c \int dE' \frac{A_1^c(E', E) A_2^{c*}(E', E)}{E - E' + i0} = \sum_c \mathrm{P.v.} \int dE' \frac{A_1^c(E', E) A_2^{c*}(E', E)}{E - E'} - i\pi \sum_{c(\mathrm{open})} A_1^c(E) A_2^{c*}(E), \tag{10}$$

where $A_1^c(E) \equiv A_1^c(E, E)$. Thus, the effective Hamiltonian for the $\mathcal{P}$ space (11) takes the form

$$\mathcal{H}(E) = H_{\mathcal{P}\mathcal{P}} + \Delta(E) - \frac{i}{2}W(E). \tag{11}$$

The resulting dynamics generated by the effective Hamiltonian (11) contains a usual $\mathcal{P}$-space contribution, which we identify here with the traditional SM corrected by the virtual "off-shell" excitations into the continuum via the self-energy

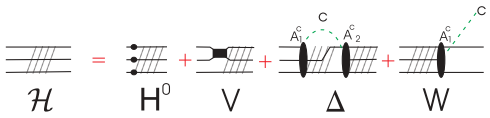

FIG. 1. (Color online) Diagrammatic equation for the full Hamiltonian corresponding to the dynamics in the $\mathcal{P}$ space, Eq. (11). Parts H° and V on the figure indicate the one- (s.p. energies) and two-body parts of the internal Hamiltonian $H_{\mathcal{PP}}$.

term,

$$\langle 1|\Delta(E)|2\rangle = \sum_c \text{P.v.} \int dE' \frac{A_1^c(E', E)A_2^{c*}(E', E)}{E - E'}, \quad (12)$$

and supplemented by the anti-Hermitian term,

$$\langle 1|W(E)|2\rangle = 2\pi \sum_{c(\text{open})} A_1^c(E)A_2^{c*}(E), \quad (13)$$

which represents the irreversible departure into $\mathcal{Q}$ space (i.e., decays); see Fig. 1. The term W, which comes from the poles in integration (9), has a factorized form, which is shown in the following to relate to conservation of probability and unitarity of the scattering matrix. The amplitudes $A^c(E)$ here represent on-shell processes that depend only on one energy parameter and correspond to real decays with energy conservation, $E' = E$. These poles in integration appear only when running energy E is above the decay threshold E_c for a channel c. The channels where decays are allowed are referred to as open. At $E \to E_c + 0$ the amplitudes A_1^c vanish because of the kinematic factors implicitly included in their definition.

B. Scattering matrix and unitarity

The "outside" view from the reaction side of the problem is equally important. In accordance with general scattering theory, the transition matrix,

$$T^{cc'}(E) = \sum_{12} A_1^{c*}(E) \left(\frac{1}{E - \mathcal{H}(E)}\right)_{12} A_2^{c'}(E), \quad (14)$$

describes the process that starts in the entrance channel c' with amplitude $A_2^{c'}$ originated from the interaction $H_{\mathcal{PQ}}$, continues through internal propagation within the $\mathcal{P}$ space driven by the non-Hermitian energy-dependent effective Hamiltonian (11) (with all excursions into $\mathcal{Q}$ space included), and ends by exit to the channel c described by the amplitude $A_1^{c*}(E)$. The scattering matrix can be written as

$$S^{cc'}(E) = \exp(i\xi_c)\{\delta^{cc'} - 2\pi i T^{cc'}(E)\}\exp(i\xi_{c'}). \quad (15)$$

The additional phase shifts $\xi_c(E)$ describe the potential scattering or a contribution of remote resonances outside of the valence space of the model. The correct normalization of the transition and scattering matrices can be checked by the comparison with perturbation theory.

The factorized nature of the non-Hermitian contribution to the effective Hamiltonian is the key for conserving the unitarity of the S matrix [24]. This can be demonstrated by considering the propagator for the effective Hamiltonian,

$$\mathcal{G}(E) = \frac{1}{E - \mathcal{H}}, \quad (16)$$

generated from the unperturbed propagator for the full Hermitian part,

$$G(E) = \frac{1}{E - H_{\mathcal{PP}} - \Delta(E)}. \quad (17)$$

With $W = 2\pi \mathbf{A}\mathbf{A}^{\dagger}$, where $\mathbf{A}$ represents a channel matrix (a set of columns of vectors A_1^c for each channel c), we iterate the Dyson equation

$$\mathcal{G} = G - (i/2)GW\mathcal{G} \quad (18)$$

and, owing to the factorized form of W, come to

$$\mathcal{G} = G - i\pi G\mathbf{A}\frac{1}{1 + i\pi \mathbf{A}^{\dagger}G\mathbf{A}}\mathbf{A}^{\dagger}G, \quad (19)$$

which is called the Woodbury equation in the mathematical literature.

The transition matrix, $T = \mathbf{A}^{\dagger}\mathcal{G}\mathbf{A}$, can then be written with the aid of the matrix $R = \mathbf{A}^{\dagger}G\mathbf{A}$, which is analogous to the R matrix of standard reaction theory. The unitarity of the S matrix follows directly from these equations (see also [25]):

$$T = \frac{R}{1 + i\pi R}, \quad S = \frac{1 - i\pi R}{1 + i\pi R}. \quad (20)$$

C. Energy dependence and resonances

The effective Hamiltonian of Eq. (11) is energy dependent: At each scattering energy E its running eigenvalues are complex numbers $\mathcal{E}_{\alpha}(E)$. This highlights the structure in Eq. (3): that the eigenstate is a superposition of internal states and asymptotic decay states that have the right energy. The relatively small, and numerically tractable, dimension of basis states, in exchange for non-Hermiticity and energy dependence, is a noteworthy advantage of this method as compared to direct discretization of the continuum used in other approaches.

The eigenvalue problem involving a complex matrix of a general form requires finding two sets of adjoint eigenvectors: right, $|\alpha\rangle$, and left, $\langle\tilde{\alpha}|$. They satisfy

$$\mathcal{H}|\alpha\rangle = \mathcal{E}_{\alpha}|\alpha\rangle \quad \text{and} \quad \langle\tilde{\alpha}|\mathcal{H} = \mathcal{E}_{\alpha}^{*}\langle\tilde{\alpha}|. \quad (21)$$

The left and right eigenstates correspond to time-reversed motions; they no longer have to coincide because the $\mathcal{T}$ invariance in the internal space is broken by irreversible decays. The global symmetry with respect to the direction of time is, however, maintained by the full Hamiltonian, which includes the products of reactions. As a result, the left and right eigenstates have the wave functions interrelated by complex conjugation, which is the time-inversion operation. The Hermitian conjugation of the Hamiltonian switches the roles of left and right; the same effect can be reproduced by selecting an advanced propagator boundary condition

in (5) discussed earlier. The biorthogonality relation is given by $\langle\tilde{\alpha}|\beta\rangle = \delta_{\alpha\beta}$; similarly, the expectation value of an operator X is $\langle\tilde{\alpha}|X|\beta\rangle$. These properties, the formalism of CSM, and its interpretation become transparent in the one-body problem discussed in Sec. III A; for further notes on this topic we refer to Ref. [26].

There are various interpretations of the eigenvalues $\mathcal{E}_\alpha(E)$ of Eq. (6). Only for bound states below all decay thresholds is a condition $\mathcal{E}_\alpha(E) = E$ satisfied since $W = 0$. With nonzero W, the eigenvalues of the effective Hamiltonian are in general complex,

$$\mathcal{E}_\alpha(E) = E_\alpha(E) - \frac{i}{2}\Gamma_\alpha(E), \tag{22}$$

describing the quasistationary states. These resonances and their widths $\Gamma_\alpha \geqslant 0$ satisfy the Bell-Steinberger relation

$$\langle\tilde{\alpha}|W|\alpha\rangle = \Gamma_\alpha, \tag{23}$$

where the left-hand side can be expressed through the amplitudes A_1^c transformed to the biorthogonal basis of quasistationary states $|\alpha\rangle$.

The continuation of the original problem to the lower part of the complex energy plane, $E \to \mathcal{E} = E - (i/2)\Gamma$, allows the condition

$$\mathcal{E}_\alpha(\mathcal{E}) = \mathcal{E}. \tag{24}$$

The complex energy roots here can be identified with the poles of the scattering matrix (14), and the eigenvectors with many-body resonant Siegert states [27] since by construction the eigenstate (3) is a regular function with outgoing asymptotics. One can also use the Breit-Wigner approach [28] and identify resonances differently, with a condition

$$\mathrm{Re}[\mathcal{E}_\alpha(E)] = E, \quad \Gamma_\alpha = -2\mathrm{Im}[\mathcal{E}_\alpha(E)]. \tag{25}$$

In the limit of small imaginary part (narrow resonances), both definitions are equivalent. However, in general the difficulty in parametrizing the resonance width and centroid energy is related to the nonexponential character of decay caused by the energy dependence of the Hamiltonian parameters. Wide resonances cover broad regions of energy and therefore are particularly affected by this dependence. This leads to the nongeneric and asymmetric shape of the resonance cross section, which makes standard Breit-Wigner or Gaussian parametrizations inappropriate.

With either definition, Eqs. (24) or (25) for resonant states are complicated sets of nonlinear equations. In some cases [7] the condition (24) may lead to unphysical solutions. For the realistic calculations shown in Sec. IV we select the Breit-Wigner definition (25) and implement an iterative approach, starting from the energy determined by the conventional SM with $W = 0$. Although it is convenient to express the solutions in terms of resonant states, the parameters are definition dependent and become misleading for broad states or in the case of overlapping resonances when interference is important. In these cases one should turn to the observable scattering cross section determined by the S matrix of Eq. (15). The computation of the scattering cross section is a problem of matrix inversion, which is linear in accordance with physical principles, but it has to be done at each energy, which can make this task numerically unstable for narrow resonances. The cross sections can be calculated using the R matrix of Eq. (20) and the Woodbury equation, in which case complex arithmetic can be avoided. We will see complementary pictures that can be obtained by calculating the cross section and via resonance parameters coming from the diagonalization of the effective Hamiltonian in the example shown in Sec. IV.

III. FROM HAMILTONIAN TO DYNAMICS

The derivation just used is based on the decomposition of the full Hamiltonian, Eq. (4). Another useful classification traditional to the SM is by the type of many-body processes it can generate. At this stage we restrict ourselves to one- and two-body interactions and limit the space $\mathcal{Q}$ by the states with only one or two nucleons in the continuum. The typical SM limitations by few valence shells are imposed on the intrinsic space $\mathcal{P}$. In this framework we define the full Hamiltonian and discuss processes associated with each of the terms.

Our discussion here, however, does not touch the lack of knowledge of the effective interaction. Although sophisticated methods of deriving the effective interactions have been suggested [22,29], the best results and the most predictive power in the conventional SM come from the phenomenological interactions, such as USD [30], fitted to experimental data. The situation becomes increasingly more complicated when effective interactions involving the continuum are to be used [26]. In this work we identify the internal interaction $H_{\mathcal{PP}}$, together with the Hermitian self-energy term Δ included, with a SM Hamiltonian of the standard form

$$H_{\mathcal{PP}} + \Delta = \sum_j \epsilon_j b_j^\dagger b_j + \frac{1}{4}\sum_{j_1 j_2 j_3 j_4} V(j_1 j_2; j_3 j_4) b_{j_1}^\dagger b_{j_2}^\dagger b_{j_3} b_{j_4}. \tag{26}$$

The parameters, s.p. energy levels and antisymmetrized two-body matrix elements, are known from fits to experimental data, such as found in Ref. [30] (see also the review in Ref. [2]), and are available from interaction libraries, such as that of Ref. [31]. The energy dependence of these parameters that comes from $\Delta(E)$ is ignored here since it has not been included in the fitting process. As demonstrated in the following this dependence is weak and $\Delta(E)$ is a smooth function of energy. Defining the internal Hamiltonian in this way we guarantee that below thresholds the CSM provides results identical to the well-established SM with effective interactions. Above thresholds, the SM interactions were fitted to experimental data using R-matrix analysis, which identifies interactions (26) in the same way [Eq. (20)]. The consistent readjustment of SM interaction parameters by taking into account the energy dependence of the Hermitian part is beyond the scope of this paper but remains a subject of future work.

In this work we assume that the Hamiltonian describing the motion of nucleons in the continuum is purely single-particle:

$$H_{\mathcal{Q}\mathcal{Q}} = \sum_j \int d\epsilon \epsilon b_j^\dagger(\epsilon) b_j(\epsilon). \tag{27}$$

The asymptotic one- and two-particle continuum states considered in this work are antisymmetrized products of internal eigenstates α of the residual nucleus and the wave function(s) of particle(s) in the continuum. The states in one-body channels,

$$|c, E\rangle = b_j^\dagger(\epsilon)|\alpha; N-1\rangle, \quad E = E_\alpha + \epsilon, \tag{28}$$

are labeled by energy E and the discrete channel index c, which combines the s.p. quantum numbers j and characteristics α for the eigenstate of an $(N-1)$-particle daughter system.

The assumption (27) allows one to express similarly the two-nucleon channel states,

$$|c; E\rangle = b_j^\dagger(\epsilon) b_{j'}^\dagger(\epsilon')|\alpha; N-2\rangle, \tag{29}$$

characterized by the combined total energy $E = E_\alpha + \epsilon + \epsilon'$ of the daughter energy E_α and energies of emitted nucleons in s.p. states j and j'. Here the channel c contains in addition information on the continuous relative energy distribution between emitted particles. Within this work we do not consider cases when both particles in the continuum are charged; thus the assumptions in Eqs. (27) and (29) are sufficient. The generalization for bound states of two particles in the continuum is relegated to the next stage.

A. Single-particle decay and resonances

Now we need to define the interaction $H_{\mathcal{P}\mathcal{Q}} + H_{\mathcal{Q}\mathcal{P}}$ responsible for coupling of intrinsic space with the continuum. We start with the one-body part and associate it with some potential V assuming this potential to be spherically symmetric.

We first treat a pure s.p. problem of a particle moving in the mean field or independent particle shell model. The generalization covering all s.p. channels in a many-body environment is straightforward and is discussed in what follows. Of course, this subject is extensively covered by textbooks [32–34]. The purpose of the formulation presented here is to emphasize the conceptual similarity between the full CSM and its trivialized version represented by a single particle in a potential. The notions and definitions of resonances, scattering matrix and its poles, time reversal properties, and non-Hermiticity already appear in this simplest case. This section also highlights some technical details used later for the s.p. part in the full CSM, including the generic threshold behavior of the decay amplitudes.

In the coordinate representation the Schrödinger equation for the radial part of the s.p. wave function,

$$\langle \mathbf{r}|b_j^\dagger|0\rangle = [Y_l \chi]_j \frac{u_j(r)}{r}, \tag{30}$$

where Y_l and χ represent the angular and spin parts coupled to total angular momentum j, is

$$\left\{ -\frac{d^2}{dr^2} + \frac{l(l+1)}{r^2} + 2\mu \left[V(r) + e^2 \frac{Zz}{r} \right] \right\} u_j(r) = k^2 u_j(r), \tag{31}$$

where $k^2 = 2\mu\epsilon$, μ is the reduced mass, and z and Z are charges of the particle and of the residual nucleus, respectively. The spin-orbit part can be included here by assuming that the potential $V(r)$ depends on l and the spin orientation, which in our notation are hidden in the s.p. index j.

For Eq. (31) with $V(r) = 0$, we have the regular, $F_l(kr)$, $F_l(0) = 0$, and the irregular, $G_l(kr)$, solutions as Coulomb wave functions with the charge parameter $\eta = \mu e^2 Zz/k$. For a neutral particle, $z = 0$, the regular and irregular solutions can be expressed in terms of spherical Bessel and Neumann functions,

$$F_l(kr) = kr j_l(kr), \quad G_l(kr) = -kr n_l(kr). \tag{32}$$

The two independent solutions are related by the Wronskian,

$$G_l \frac{d}{d(kr)} F_l - F_l \frac{d}{d(kr)} G_l = 1. \tag{33}$$

Thus, the $\mathcal{Q}$-space states are energy-normalized regular solutions,

$$\langle \mathbf{r}|j;\epsilon\rangle = \langle \mathbf{r}|b_j^\dagger(\epsilon)|0\rangle = [Y_l\chi]_j \sqrt{\frac{2\mu}{\pi k}} \frac{F_l(kr)}{r}. \tag{34}$$

Following the definition in Eq. (8), we obtain the s.p. decay amplitude of

$$\begin{aligned} a_j(\epsilon_j, \epsilon) &= \langle j|H_{\mathcal{P}\mathcal{Q}} - \epsilon|j;\epsilon_j\rangle \\ &= \sqrt{\frac{2\mu}{\pi k_j}} \int_0^\infty dr F_l(k_j r)[V(r) + \epsilon_j - \epsilon] u_j(r). \end{aligned} \tag{35}$$

A positive-energy internal state $u_j(r)$ decays with the width $\gamma_j = 2\pi a_j^2$ determined by the this equation; under this choice of phases, the decay amplitudes are real.

This result for the decay width can be reproduced through the equivalent consideration of the on-shell scattering process. Let us introduce incoming and outgoing (Coulomb) waves $O_l^\pm(r) = G_l(r) \pm i F_l(r)$. Consider a resonant state u_j. (Through the rest of this section we concentrate on a state with a given set of s.p. quantum numbers j, so we will omit this subscript in the notation; the orbital momentum subscript l, which is a part of the combined index j, is also omitted.) The state u can be normalized as a discrete state when the decaying component that obeys the Siegert [27] outgoing wave boundary condition,

$$\lim_{r\to\infty} u(r) = \mathcal{N} O^+(kr), \tag{36}$$

is neglected. Then the outgoing flux normalized by velocity determines the decay width

$$\gamma = 2\pi a^2 = \frac{k}{\mu}|\mathcal{N}|^2. \tag{37}$$

It follows from here that the asymptotics of the decaying states are given by the decay amplitude,

$$\lim_{r\to\infty} u(r) = -\sqrt{\frac{2\pi\mu}{k}}a(\epsilon)O^+(kr), \tag{38}$$

where we selected a phase to be consistent with the previous definition. Using the Wronskian relations, the outgoing part can be extracted from the wave function u_j, leading to

$$a(\epsilon) = -\sqrt{\frac{1}{2\pi\mu k}}\left(u\frac{dF}{dr} - F\frac{du}{dr}\right)\Big|_{r\to\infty}. \tag{39}$$

This equation is identical to Eq. (35) since the Schrödinger equation (31) that must be used to determine the outgoing component guarantees that

$$\frac{d}{dr}\left(u\frac{dF}{dr} - F\frac{du}{dr}\right) = -2\mu F V(r)u(r), \tag{40}$$

where F is any of the Coulomb wave functions.

The eigenstate wave function in the asymptotics can be expressed via the s.p. scattering phase shift, $u_j(\epsilon) \sim \cos(\delta_j)F_l + \sin(\delta_j)G_l$. The related S matrix then can be found as

$$S = \exp(2i\delta) = \frac{u\frac{d}{dr}O^- - O^-\frac{d}{dr}u}{u\frac{d}{dr}O^+ - O^+\frac{d}{dr}u}\Bigg|_{r\to\infty}, \tag{41}$$

which is consistent with definitions (14) and (15). The poles of the scattering matrix correspond to the condition of the regular wave function with the outgoing wave in asymptotics. Just as in the general case in Sec. II, this cannot be satisfied at real energy, whereas if the problem is taken into a complex energy plane, $k \to \kappa = k - i\varkappa$ and $\epsilon \to e = \epsilon - i\gamma/2$, the discrete set of solutions emerges. Thus, the resonance energy ϵ and the width γ can be defined as real and imaginary parts, respectively, of the complex energy, which is the pole of the scattering matrix. Consistent with the general theory, the time-reversed problem is physically equivalent; the boundary condition then is that the wave function be regular at the origin and represent an incoming wave in asymptotics. This is a $\mathcal{T}$-reversed state, with the corresponding "left" momentum eigenvalue $\tilde{\kappa}$ being related to that of the "right" eigenstate as $\tilde{\kappa} = -\kappa^*$. This agrees with the symmetry properties of the S matrix,

$$S(\kappa) = S^*(-\kappa^*) = S^{-1}(-\kappa), \tag{42}$$

and ensures that the left and right energy eigenvalues are complex conjugate.

Numerically, the decay amplitudes can be calculated directly from (35) or (39); it has been demonstrated in Ref. [35] for proton emitters that these methods are equally effective in practice. The effective non-Hermitian s.p. Hamiltonian can be solved, resulting in Gamow states via an iterative procedure based on the Green's function, similar to the approach discussed in Refs. [36,37]. Green's function is constructed for the free particle case $V = 0$ by using Coulomb functions at some momentum k_0 and the Siegert boundary conditions,

$$\mathcal{G}(r, r') = \frac{1}{k_0}F(k_0 r_<)O^+(k_0 r_>). \tag{43}$$

The $r_<$ and $r_>$ denote the smaller and the larger of r and r', respectively. The integral equation for the resonant state becomes

$$u(r) = \int_0^\infty \mathcal{G}(r, r')\left[\kappa^2 - k_0^2 - 2\mu V(r')\right]u(r')dr'. \tag{44}$$

This leads to the following equation for the radial part $u(r)$:

$$\begin{aligned} u(r) \;=\; & \frac{1}{k_0}F(r)\left\{\int_r^\infty O^+(r')\left[\kappa^2 - k_0^2 - 2\mu V\right]u(r')dr'\right\} \\ & + \frac{1}{k_0}O^+(r)\left\{\int_0^r F(r')\left[\kappa^2 - k_0^2 - 2\mu V\right]u(r')dr'\right\}. \end{aligned} \tag{45}$$

The complex momentum κ is determined self-consistently with the decay flux defined by the outgoing component in this equation.

B. Threshold behavior

The behavior of the decay width and the self-energy term $\Delta(\epsilon)$ in the vicinity of threshold is particularly important. The one-body decay is an instructive example of the CSM at work. Following the preceding definitions we evaluate

$$\int_0^\infty d\epsilon_j \frac{|a_j(\epsilon_j, \epsilon)|^2}{\epsilon - \epsilon_j + i0} = \Delta(\epsilon) - \frac{i}{2}\gamma(\epsilon) \tag{46}$$

in the vicinity of the single-particle threshold at zero energy using Eq. (35), which we decompose as

$$a_j(\epsilon_j, \epsilon) = \langle j|V|j;\epsilon_j\rangle + (\epsilon_j - \epsilon)\langle j|j;\epsilon_j\rangle. \tag{47}$$

Only the first term in (47) leads to a pole in Eq. (46). The main contribution comes from low-energy scattering states, namely in the limit when the de Broglie wavelength of the scattered particle exceeds the range of the potential. For a charged particle, the energy behavior of the amplitude (35) follows from that of the regular Coulomb function. For a neutral particle, in this limit $F_l = (kr)^{l+1}/(2l+1)!! \propto \epsilon^{(l+1)/2}$. Thus at low energies we can assume that

$$\langle j|V|j;\epsilon_j\rangle = æ_j(\sqrt{\epsilon_j})^{l+1/2}, \tag{48}$$

where the constant $æ_j$ is

$$æ_j = \frac{(2\mu)^{(l+3/2)/2}}{\sqrt{\pi}(2l+1)!!}\int_0^\infty r^{l+1}V(r)u_j(r)dr. \tag{49}$$

When the decay amplitude (47) is substituted in the integral (46) only the term $\propto æ_j^2$ contains the contribution from the pole if $\epsilon > 0$. The residue at that pole under low-energy conditions is given by Eq. (48). This term controls the appearance of decay width and the near-threshold behavior. All other contributions

can be conveniently expressed using the projection operator onto external space, $\hat{\mathcal{Q}} = \int d\epsilon_j |j\epsilon_j\rangle\langle j\epsilon_j|$. Thus,

$$\Delta(\epsilon) = \langle j| - H_{\mathcal{Q}\mathcal{Q}} - \hat{\mathcal{Q}}V - V\hat{\mathcal{Q}}|j\rangle + \epsilon\langle j|\hat{\mathcal{Q}}|j\rangle + \pi æ_j^2\Theta(-\epsilon)\epsilon^l\sqrt{-\epsilon}, \quad (50)$$

and for the imaginary part

$$\gamma_j(\epsilon) = 2\pi æ_j^2\Theta(\epsilon)\epsilon^{l+1/2}, \quad (51)$$

where Θ is the Heaviside step function. The first two terms in Eq. (50) appear as a correction to the energy because of the possible nonorthogonality between the states of $\mathcal{Q}$ and $\mathcal{P}$. They are small in any reasonably selected situation; they are identically zero in the examples shown in the following where spaces $\mathcal{P}$ and $\mathcal{Q}$ are obtained from the full numerical solution of the Woods-Saxon potential. Only the second term in (50) depends linearly on energy.

The last term in Eq. (50) appears only below threshold and represents virtual excitation into the continuum, induced by interaction. This contribution is a continuous function of energy and is also smooth except for the s-wave neutral-particle decay channel. The behavior of the self-energy $\Delta(\epsilon)$ including the s-wave cusp $\sim\sqrt{\epsilon}$ is well studied in hadron physics; it is a direct consequence of threshold unitarity (see also Refs. [33,38]). The scaling coefficient $æ_j$ that enters this expression is typically small; the same coefficient determines the energy scaling of the decay width above threshold, Eq. (51) (see Fig. 3). The behavior $\gamma \sim \epsilon^{l+1/2}$ is consistent with the phase-space volume for one-body decay. It is universal, so that, if the potential were adjusted to reproduce a certain resonance energy, then the behavior of the width as a function of resonance energy remains the same [38,39].

C. One-body channels in a many-body system

The one-body decay amplitude in a many-body system is given by the s.p. decay and the spectator overlap,

$$A_1^c(E) = a_j(\epsilon)\langle 1; N|b_j^\dagger|\alpha; N-1\rangle, \quad (52)$$

where energy of the continuum state is $E = E_\alpha + \epsilon$ and $c = \{\alpha, j\}$. This amplitude is to be directly used in the non-Hermitian effective Hamiltonian (11). Even on the level of s.p. decays, the approach outlined here goes beyond the consideration based solely on spectroscopic factors. Here the non-Hermitian part of the effective Hamiltonian is not a s.p. operator. Indeed, even s.p. decays can generate significant restructuring inside the nucleus. Effects such as shape changes or changes in pairing coherence are extremely important for the physics of nuclei far from stability. The energy dependence that was discussed earlier is another distinct feature.

Although in all calculations presented in this work we use a general form of the effective Hamiltonian, in the following we show a set of approximations that establish a correspondence with the traditional SM description of decay. For simplicity we assume that all internal s.p. states can be identified by spin and parity (i.e., the space is small enough not to include several major shells). In the case of remote thresholds, the decay amplitudes become essentially independent of energy, and the set of continuum channels $c = \{\alpha, j\}$ includes almost all possible daughter states α. The completeness in α and energy independence can be then used to simplify the non-Hermitian term that becomes diagonal,

$$\langle 1|W|2\rangle = 2\pi\delta_{12}\sum_j |a_j|^2\langle 1; N|b_j^\dagger b_j|1; N\rangle. \quad (53)$$

As a result, W is then a s.p. operator that assigns a width (37) to each s.p. state j coupled to the continuum, $W = \sum_j \gamma_j b_j^\dagger b_j$. The same picture emerges when the residual SM interaction is weak. Then s.p. motion masters the dynamics, and the sum over daughter systems α is dominated by a single term. This again leads to Eq. (53), that is energy dependent: $W(E) = \sum_j \gamma_j(E) b_j^\dagger b_j$. The operator W here can be conveniently combined with the SM Hamiltonian just by introducing complex s.p. energies for unstable orbitals in the mean field (for a simple instructive example see Ref. [40]). Another point to be mentioned here is related to the treatment of the non-Hermitian part. In the full CSM diagonalization, virtual transitions to the continuum and real decays influence the internal structure. This is particularly important at strong continuum coupling when coherence with respect to decay leads to the super-radiance phenomenon [7,25,41].

The second situation leading to the SM picture is the limit of weak continuum coupling when the matrix W can be treated perturbatively. In the lowest order, decays do not affect the internal state and we can solve the Hermitian problem first to obtain a many-body state $|\alpha\rangle$ with the width given by the expectation value

$$\Gamma_\alpha = \langle\alpha|W|\alpha\rangle = \gamma_j \Upsilon_j(\alpha). \quad (54)$$

This expresses a many-body decay width as a product of the s.p. width and the spectroscopic factor $\Upsilon_j(1) = \langle 1; N|b_j^\dagger b_j|1; N\rangle$.

D. Two-nucleon emission

A two-body decay channel state is fixed by an $N-2$ nucleus in its eigenstate α and a state of two nucleons in the continuum, Eq. (29). These states are characterized by the combined total energy $E = E_\alpha + \epsilon + \epsilon'$ of the daughter energy E_α and energies of emitted nucleons in s.p. channels j and j', the total angular momentum, and the isospin of the emitted pair. Unless we are dealing with a bound two-particle continuum state, the channel, besides total energy E, has another continuous index describing the energy distribution between the particles.

As was done earlier, the two-body transition amplitude is generated by the matrix element $\langle 1|H|c; E\rangle$ of the original Hamiltonian. Two different contributions can be identified: "direct" and "sequential" (Fig. 2). The one-body part of the total Hamiltonian H defined here cannot contribute to the direct decay vertex $1 \to \alpha + j + j'$. The two-body interaction responsible for this direct transition is discussed in the

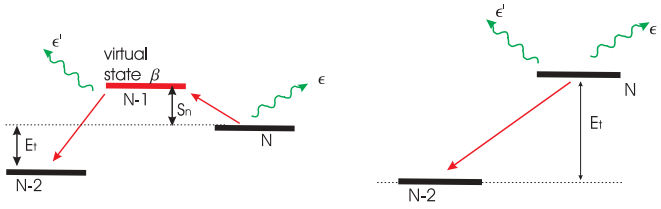

FIG. 2. (Color online) Diagrams for two-body decays: sequential (left part) and direct (right part).

following. Even without two-body interactions, the "dressed" vertex is not zero since the $N-2$ daughter state is a part of the virtual cloud of the $N-1$ system to which one-body transitions are allowed. Such a second-order perturbative sequential mechanism of decay is possible regardless of whether the one-body channel is open or closed. A similar approach and classification of processes has been recently discussed in the context of two-proton radioactivity [42,43], where on one hand the case is complicated by being a three-body Coulomb problem [44], while on the other hand extremely weak decays do not affect the internal nuclear structure, allowing the use of the traditional real-energy SM [43].

1. Sequential decay

The dressed s.p. vertex for two-nucleon emission $\langle 1|H|c;E\rangle$ can be calculated with the help of Eq. (3) and solution (7),

$$A_1^c(E_c,E) = \sum_\beta \frac{A_1^{\{\beta j\}}(E_\beta+\epsilon,E)\quad A_\beta^{\{\alpha j'\}}(E_\alpha+\epsilon',E_\beta)}{E_\beta-E_\alpha-\epsilon'} - (\{\epsilon,j\}\leftrightarrow\{\epsilon',j'\}). \tag{55}$$

Assuming that internal and external s.p. states are orthogonal and using the one-body decay amplitude (52) for the second-order process that takes place via a virtual state β being suppressed by the energy barrier, we obtain

$$A_1^c(E) = \sum_\beta a_j(\epsilon)a_{j'}(\epsilon') \times\left(\frac{\langle 1|b_j^\dagger|\beta\rangle\langle\beta|b_{j'}^\dagger|\alpha\rangle}{S_\beta+\epsilon} - (\{\epsilon,j\}\leftrightarrow\{\epsilon',j'\})\right), \tag{56}$$

where we are considering on-shell decay so that the initial state with energy $E=E_\alpha+\epsilon+\epsilon'$ undergoes a transition via the intermediate state with energy $E_\beta+\epsilon$. This is reflected in the denominator, $S_\beta+\epsilon=E_\beta-E+\epsilon$, where S_β stands for the separation energy from the intermediate system. Since $c=\{j\epsilon,j'\epsilon',\alpha\}$ here contains a continuous index, the summation over channels is expressed as

$$\langle 1|W(E)|2\rangle = \pi\sum_{\alpha,j,j'}\int d\epsilon d\epsilon' \times\delta(E-E_\alpha-\epsilon-\epsilon')A_1^c(E)A_2^{c*}(E). \tag{57}$$

To avoid double-counting from fermion permutation we included a factor of 1/2 while making the domain of integration symmetric. Equation (57) may contain poles in open one-body channels corresponding to real states of an $N-1$ system through which the two-body decay process can proceed. Such processes can be viewed as a second-order correction to the one-body decay via the daughter state β as a resonant state. Here we discuss only the off-shell contribution. An example of sequential decay is shown in Fig. 2.

The calculation of the non-Hermitian term W in the most general case was carried out numerically in the examples shown in Sec. IV. Here we illustrate the case of a weakly decaying state $|\alpha_i\rangle$ when the decay width can be approximated by the diagonal element, $\Gamma=\langle\alpha_i|W|\alpha_i\rangle$. In this limit the problem is close to that of sequential decay discussed in Refs. [43,45].

Taking into account the direct and exchange contributions to Eq. (56), assuming spherical symmetry, and performing the summation over magnetic quantum numbers, we obtain two spectroscopic factors,

$$\Upsilon^{\rm d}=\delta_{jj'}\delta_{\beta\beta'}\frac{|\langle\alpha_f||b_j||\beta\rangle\langle\beta||b_j||\alpha_i\rangle|^2}{(2\alpha_i+1)(2\beta+1)} \tag{58}$$

and

$$\Upsilon^{\rm x} = (-1)^{\beta+\beta'}\begin{Bmatrix}\alpha_i & j & \beta'\\ \alpha_f & j' & \beta\end{Bmatrix} \times\frac{\langle\alpha_f||b_{j'}||\beta'\rangle^*\langle\beta'||b_j||\alpha_i\rangle^*\langle\alpha_f||b_j||\beta\rangle\langle\beta||b_{j'}||\alpha_i\rangle}{2\alpha_i+1}, \tag{59}$$

where here (and in the following) we use the Greek index of the many-body state as a symbol of angular momentum. The reduced matrix elements are defined as in [32]. The total width in the channel $|\alpha_i\rangle\to|\alpha_f\rangle$ is given by

$$\Gamma = \frac{1}{2\pi}\int d\epsilon d\epsilon'\delta(E_t-\epsilon-\epsilon')\sum_{\beta\beta' jj'}\gamma_j(\epsilon)\gamma_{j'}(\epsilon') \times\left(\frac{\Upsilon^{\rm d}}{(S_\beta+\epsilon)^2}+\frac{\Upsilon^{\rm x}}{(S_\beta+\epsilon')(S'_\beta+\epsilon)}\right). \tag{60}$$

As an illustration, we discuss a case of the $0^+\to0^+$ two-neutron decay. Here $\Upsilon^{\rm x}=\Upsilon^{\rm d}\equiv\Upsilon$, and we can view a full width as a sum of partial widths that depend on the final state α_f and intermediate state β. The characteristic energies in the problem are the one-neutron separation energy to the state β, $S_\beta=E_\beta-E_{\alpha_i}$, and the two-neutron decay energy, $E_t=E_{\alpha_i}-E_{\alpha_f}$ (minus the two-neutron separation energy). We assume a situation with small available energy $E_t=\epsilon+\epsilon'$, when the energy scaling of the s.p. decay widths, $\gamma_j=2\pi|a^j(\epsilon)|^2\sim\epsilon^{l+1/2}$, can be used. Introducing $q=E_t/S_\beta$ we obtain

$$\Gamma_\beta(0\to0)=\Upsilon\frac{\gamma_l(E_t)\gamma_{l'}(E_t)E_t}{S_\beta^2}\mathcal{B}_{ll'}(q), \tag{61}$$

which includes the phase-space integral

$$\mathcal{B}_{ll'}(q) = \frac{(2+q)}{2\pi}\int_0^1 \frac{x^{l+1/2}(1-x)^{l+1/2}}{(1+qx)^2[1+q(1-x)]}dx. \quad (62)$$

In the limit $S_n \gg E_t$ we obtain $\mathcal{B}_{ll'}(q) = B(l+3/2, l'+3/2)/\pi$, where $B(x,y)$ is a beta function. The decay rate is suppressed by the energy denominator S_β^2. The two-body decay width scales with energy as E_t^2. This is consistent with the phase-space volume estimate, $\Gamma \sim \delta^3(P_t - P)\delta(E_t - E)\Pi_i(d^3k_i/\epsilon_i)$, where P is total momentum and the product Π_i runs over the fragment indices including the daughter nucleus. For the isotropic case integrated over all angles, the width is proportional to $\gamma \sim k \sim E_t^{1/2}$ in one-body decay; the same assumptions lead to $\Gamma \sim E_t^2$ for the two-body decay (three-body final phase space).

In the opposite limit, $S_n \ll E_t$ or $q \to \infty$, we have $\mathcal{B}_{ll'}(q) = B(l-1/2, l'+1/2)/(2\pi q^2)$. This expression diverges for an s wave. The exact integration in the s-wave case gives

$$\Gamma_{\beta=1/2}(0\to 0) = \frac{\gamma_0^2(E_t)\Upsilon_\beta E_t}{4(2S_\beta + E_t)\sqrt{S_\beta(S_\beta+E_t)}}. \quad (63)$$

Note the divergence in the s-wave channel when separation energy goes to zero. The s-wave state in the intermediate nucleus β is so broad that even being slightly higher in energy it still poses no barrier for the sequential decay. The generic behavior of the isotropic decay width as a function of energy can be traced from Eq. (63), where $\Gamma \sim E_t^2$ if energy is low, $E_t \ll S_\beta$, but once energy gets above S_β the behavior changes to $\Gamma \sim \sqrt{E_t}$. This shows that the presence of the one-body resonance changes the nature of sequential decay, reflecting the one-body phase-space characteristics. For simplicity of our discussion so far the width of the intermediate state β has been ignored; however, this width is present in the realistic calculations discussed in the following.

2. *Direct decay*

Direct two-body transitions are generated by the two-body part of the Hamiltonian $H_{\mathcal{QP}}$, which takes a nucleon pair coupled to angular momentum L, $p_L = [b_j b_{j'}]_L$,from internal space $\mathcal{P}$ and transfers it to the two-body continuum $\mathcal{Q}$ (see the right part in Fig 2). The transition amplitude has the generic form

$$A_1^c(E) = a^{(j_1 j_2)}(\epsilon_1, \epsilon_2)\langle 1; N|(p_L^{(jj')})^\dagger|\alpha; N-2\rangle, \quad (64)$$

where a direct two-body transition amplitude, $a^{(j_1 j_2)}(\epsilon_1, \epsilon_2)$, is introduced [and is not to be confused with s.p. amplitudes $a^j(\epsilon)$]. This amplitude can be calculated for a given two-body interaction. For example, by assuming for simplicity a coordinate form $V^{(2)}(r, r')$, where r and r' are particle coordinates in the mean-field frame, the amplitude can be expressed following the definition of Eq. (8) and normalized free-particle states F_j as

$$\begin{aligned} a^{(j_1 j_2)}(\epsilon_1\epsilon_2) &= \langle j_1 j_2|V^{(2)}|j_1, \epsilon_1; j_2, \epsilon_2\rangle \\ &= \frac{2\mu}{\pi\sqrt{k_1 k_2}}\int_0^\infty dr dr' F_{j_1}(r)F_{j_2}(r') \\ &\quad \times V^{(2)}(r, r')u_{j_1}(r)u_{j_2}(r'). \end{aligned} \quad (65)$$

The low-energy behavior of the direct amplitude can be understood without specification of the residual interaction by taking into consideration the long-wavelength behavior of the Bessel functions associated with the regular solution, $F_l(r) \sim (kr)^{l+1}$ at $k \to 0$. The decay rate can be estimated by integration over continuous channel variables as in Eq. (57):

$$\Gamma \sim \int |a^{(j_1 j_2)}(\epsilon_1\epsilon_2)|^2\delta(E_t - \epsilon_1 - \epsilon_2)d\epsilon_1 d\epsilon_2 \sim E_t^{l_1+l_2+2}. \quad (66)$$

The same answer as the one obtained for the sequential transition reflects the nature of the three-body final phase space. The direct transition however is not suppressed by the one-body energy barrier and is not related to decay amplitudes for one-body decays.

We conclude the discussion of two-body decay processes with a word of caution: The full amplitude in a given decay channel is the sum of the direct and sequential contributions and the observed width or cross section carries their interference.

IV. APPLICATIONS

A. How the method works

Before turning to the discussion of the specific results we outline the stages involved in the calculation. A special feature of our approach is the exact treatment of threshold behavior. This requires the knowledge of the topography of thresholds and therefore has to rely on the preceding solution for the daughter systems. In this way we come to problems that involve the daughter chains in their entirety. Thus, except for the case of the traditional SM, where the Hermitian Hamiltonian matrix is diagonalized separately for each nucleus, in all calculations the nuclides (or, in our examples that follow, the isotopes) are coupled by the decay chains.

The procedure starts from the closed core (specifically, ^{4}He or ^{16}O) and continues toward heavier isotopes so that the properties of all possible daughter nuclei are known prior to each new calculation. The process of calculating resonant states is iterative. We start with a given state obtained from the conventional SM. For this state we review all possible one-body and two-body decays. To determine the contribution to W from each individual one-body channel we conduct a scattering calculation where we use Eq. (35) to determine a s.p. decay amplitude. The state u_j is determined from the solution for the Woods-Saxon potential; it is then normalized as a discrete state and identified with a s.p. SM state that is involved in the process. The amplitudes for two-body sequential channels are determined using one-body amplitudes, as discussed in

Sec. III D. The diagonalization of the full Hamiltonian with the non-Hermitian part results in the next iteration for energy and width of the state under consideration. For each resonant state this process continues until convergence is reached. The Breit-Wigner definition of resonances is used so that scattering calculations are done at real energy.

By construction of the model, with $\Delta(E)$ [Eq. (11)], assumed to be included in the adjusted SM Hamiltonian with neglected energy dependence, bound levels coincide with those in the standard SM. For unbound states, this choice makes our internal propagator equivalent to the R matrix used in spectroscopic analysis of experimental data. Therefore this design is most suitable for the effective extraction of interaction parameters from experiment.

The continuum coupling restructures internal states, and energies of resonances above the decay threshold deviate from the SM predictions. For narrow states and well-separated resonances, the resulting effect is small. The spherical shape of the semimagic system is stable; in addition, strong collective pairing reduces the effect of decays onto internal structure in these particular examples. Hence, for s.p. decays [case (a) in Table I], the use of the spectroscopic factor approximation discussed in Sec. III C is rather good. Here we are far from a strong coupling to the continuum [12,25,49,50], which might cause an internal phase transition with formation of broad (super-radiant) and very narrow (trapped) states. In nuclear physics this phenomenon separates compound and direct reactions [25,51,52]. A trace of this effect is seen in Table I, where decaying states have their resonant energy shifted from the SM prediction, with the lowest states of the given quantum numbers being pushed into the continuum [7].

The cross-section calculations follow directly the formalism outlined in Sec. II B. In these calculations we use the same set of decay channels, thereby, because of unitarity, ensuring proper treatment of the flux loss to nonelastic channels. The large-scale repetitive matrix inversion and instability in the vicinity of the poles present a significant technical challenge. In this work we employed a new numerical method that expands the unperturbed propagator (17) in the time domain using Chebyshev polynomials. The entire procedure is similar to the Lanczos technique and involves only matrix vector multiplication, which is a fast operation with sparse matrices. The resulting R matrix is then used in the Woodbury equation (19), leading to a full propagator and scattering cross section.

TABLE I. Comparison of conventional SM and CSM with data for He isotopes.[a] The first two columns indicate the mass number and spin of the state. The next three columns compare energies as follows: E(SM)— traditional shell model; E(CSM)—full CSM including two-body decay modes; E(EX)—experimental data (some of which have large uncertainties and depend on the method of analysis). The three columns to the right show decay widths: Γ(a)—CSM with one-body decay channels; Γ(CSM)—CSM with all channels and experimental reaction kinematics. The experimental data in column Γ(EX) are taken from Refs. [46–48].

A	J	E(SM)	E(CSM)	E(EX)	Γ(a)	Γ(CSM)	Γ(EX)
4	0	0	0	0	0	0	0
5	3/2	0.992	0.992	0.798	1.0	0.729	0.648
5	1/2	4.932	4.932	2.07	broad	6.00	5.57
6	0	−1.379	−1.379	−0.973	0	0	0
6	2	0.515	0.515	0.825	0	0.037[b]	0.113
6	2	4.745	4.110		4.74	4.74	
6	1	5.889	5.889		6.98	6.98	
6	0	11.088	10.183		13.85	13.85	broad
7	3/2	−1.016	−1.016	−0.529	0.091	0.126	0.15
7	1/2	2.240	2.240	2.1	4.45	2.93	2
7	5/2	2.85	2.850	2.39	3.49	4.03	1.99
7	3/2	4.495	4.521	(5.3)	5.79	(6.77)	(4)
7	3/2	10.223	9.304		15.24	15.24	
8	0	−3.591	−3.591	−3.112	0	0	0
8	2	0.19	0.196	0.48	0.336	0.238	0.8
8	1	2.427	2.427		4.40	3.37	
8	0	6.376	5.974		11.5	11.5	
8	2	6.882	6.740		12.13	12.13	
9	1/2	−1.992	−1.992	(−1.84)	0.543	(0.334)	0.1
9	3/2	2.805	2.805	(−0.69)	5.12	(0.568)	0.7
10	0	−1.649	−1.649	−2.04	0.073	[c]	0.3

[a]All numbers in MeV; energies are measured from the ground state of ^{4}He.

[b]This result includes one- and two-body decay modes; single-particle decay width is 6 keV (see text).

[c]The state is likely to decay via two-body mode thorough the process dominated by $l = 0$ transitions involving states from the *sd* shell. These configurations are not a part of our model.

B. Helium isotopes

For the chain of helium isotopes from ^{4}He to ^{10}He, the results are summarized in Table I. The internal valence $\mathcal{P}$ space contains two s.p. levels, $p_{3/2}$ and $p_{1/2}$; the α-particle core is kept inert. The effective interaction within this model space and s.p. energies are borrowed from Refs. [53,54]. Without additional terms, this would be merely a conventional SM, leading to the bound states that are listed as E(SM) in Table I (with all energies being measured from the ground state of ^{4}He).

The one-body part of the coupling Hamiltonian $H_{\mathcal{PQ}}+H_{\mathcal{QP}}$ is defined using the Woods-Saxon potential. The parameters of the potential are $V = 46.92$ MeV, $V_{\rm SO} = 28.9$ MeV; radius $R = 2.064$ fm and diffuseness 0.7 fm are the same for the central and spin-orbit Woods-Saxon density form factors. In our calculations the potential depth was adjusted to retain the resonant nature of one-body reactions. As discussed in Sec. III A, the internal wave functions of this potential are then used to calculate the decay amplitudes. It should be stressed that modification of the mean field given by the interaction $H_{\mathcal{PQ}} + H_{\mathcal{QP}}$ from isotope to isotope is a subject of separate investigation; generally, only in clear s.p. cases is adjustment of depth a good approach for determining the mean field. In our earlier investigations [8], such mean-field modifications were not always used and this typically led to smaller widths.

As already discussed, at low energies the s.p. decay widths behave according to Eq. (51). In our case this approximate behavior for the $l = 1$ partial wave is $\gamma(\epsilon) = 0.834\,\epsilon^{3/2}$ MeV

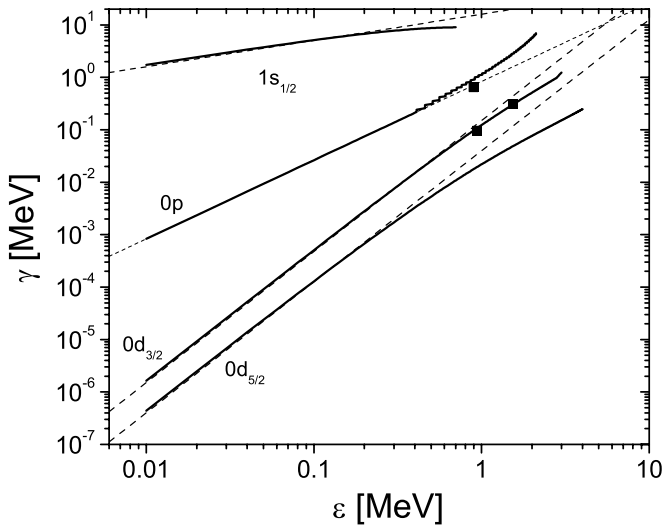

FIG. 3. Single-particle decay width as a function of resonance energy for the p- and sd-shell models. The solid lines represent the results of the reaction calculations based on the Woods-Saxon potential appropriate for the corresponding case (helium or oxygen) discussed in the text. One experimental point on the p-state line corresponds to the ground-state $3/2^-$ resonance in ^{5}He ($\epsilon = 0.895$ MeV and $\gamma = 648$ keV). Two points for the $d_{3/2}$ state correspond to the experimentally known $3/2^+$ resonances in ^{17}O ($\epsilon = 0.941$ MeV and $\gamma = 98 \pm 5$ keV) and ^{19}O ($\epsilon = 1.540$ MeV and $\gamma = 310 \pm 30$ keV [55]). The near-threshold power-law fits of Eq. (51) are shown with dashed lines.

for both $p_{3/2}$ and $p_{1/2}$ states (see Fig. 3). Higher above the decay threshold, the concept of decay width as an observable quantity becomes ambiguous; however, one can trace the poles of the scattering matrix, which sharply dive down into the complex plane, while the real part of the pole remains finite. This important property prohibits adjustment of the potential depth for the high-lying s.p. resonances. An example of this situation is given by the $1/2^-$state in ^{5}He, which in the compilation [46] of 1988 (and also used in our work [8]) appeared at an energy of nearly 5 MeV above the threshold. The $0p_{1/2}$ resonance pole cannot have such a high value for its real part. Thus adjustment of the mean field is neither possible nor warranted in this situation.

The results of the CSM calculation are shown in Table I. Here we primarily concentrate on the s.p. channels owing to their close relation to experimental data. Unlike the case of oxygen (see Sec. IV C), and the results reported in Ref. [8], we deliberately present here a somewhat simpler study and trace results in detail. The "Borromean" ^{6}He nucleus is the only case discussed in the following where two-body decays appear to be important. The sequential two-body decay as a second-order process built on one-body amplitudes involves no additional parameters. In our earlier work [8], the roles of direct and sequential decay were analyzed for the helium chain under different assumptions for the interactions and with the older experimental data available at that time.

The results of our calculations for resonance energies are shown as E(CSM) in Table I. Experimentally known energies of corresponding states or resonances are listed in the E(EX) column. On the right side of the table we show the decay widths determined using the Breit-Wigner definition. The column Γ(a) corresponds to the calculation that includes only one-body channels and uses reaction characteristics fully determined by the CSM. The column Γ(CSM) shows the full CSM results. Because the results are sensitive to scattering kinematics the full calculation is carried out at experimentally observed Q values, where available. The full calculation also includes a case of sequential two-body decay as discussed in the following.

Next we comment on some of the features of the results.

(i) The ground states of ^{4,6,8}He are nucleon-stable, in agreement with experiment.

(ii) The correspondence with previously known results is preserved. For example, the ^{7}He ground state $3/2^-$ has only a single open channel for decay into the ground state of ^{6}He with a Q value of 0.364 MeV; the spectroscopic factor for this particle removal is $\Upsilon = 0.498$. A calculation with the Woods-Saxon potential adjusted to produce a 3/2 resonance at this energy gives a width of 0.183 MeV; together with the spectroscopic factor this amounts to a 91-keV width, which is consistent with the 91-keV width obtained in a full calculation. As proven in Sec. III A, perturbation theory, which is equivalent to the use of the conventional SM with the spectroscopic factor, is valid, provided that the decay width (perturbative term) is small. Another case is a broad $3/2^-_2$ state in this nucleus; coupling through the

continuum mixes all $3/2^-$states, making the use of a perturbative approach invalid. We emphasize here that the CSM does not use external spectroscopic factors.

(iii) The two-neutron decay of the 2^+state in ^{6}He is of particular interest. Because of the extreme sensitivity of the decay width to the reaction kinematics, we conduct this discussion by assuming observed energies. The latest experimental data show the 2^+ state to be only 27 keV above the single-neutron decay threshold. At this energy, the potential calculation gives a width of about 3.7 keV. The spectroscopic factors of $\Upsilon_{1/2} = 0.166$ and $\Upsilon_{3/2} = 1.670$ lead to a total single-nucleon decay width of about 6.3 keV, consistent with the CSM calculation in Table I. This result is significantly smaller than the experimental value, emphasizing the dominant role of two-neutron decay, which is equivalent to α decay in this example. The sequential two-body decay is primarily determined by the kinematic phase-space integral, where the sequential two-body process proceeds via an intermediate state β,

$$\gamma_{jj'}(Q) = \frac{1}{2\pi}\int_0^Q d\epsilon \frac{\gamma_j(\epsilon)\gamma_{j'}(Q-\epsilon)}{(\epsilon + E_\beta - E_\alpha)^2 + \Gamma_\beta^2/4}. \quad (67)$$

In this equation the intermediate state is assumed to be an isolated resonance so that the s.p. propagator can be represented by a Lorentzian. The transition through the intermediate $1/2^-$ resonance in ^{5}He is too weak because of the high barrier. The Q value of 0.825 MeV and separation energy $S = 1.243$ MeV lead to the width $\gamma_{jj'}$ being less than 1 keV. Sequential two-body decay through the $\beta = 3/2^-$ state is significant: By substituting realistic kinematics into the integral (67) we obtain $\gamma_{jj} = 17$ keV. This is the result of a pure potential calculation, which has to be supplemented with spectroscopic factors and recoupling coefficients as discussed in Sec. III D. In fact, given the simplicity of this recoupling and the trivial spectroscopic factors in ^{5}He, only the afiorementioned spectroscopic factors of ^{6}He enter into the final result. The CSM calculation leads to a total width of 37 keV for the 2^+state, which can be compared with the experimental value of 113 ± 20 keV.

(iv) The results reveal information about nuclear structure and dominant decay modes. For example, for the ^{7}He isotope, the results agree with the recent experiments [47,48] and support the "unusual structure" of the $5/2^-$ state identified in Ref. [48]. Owing to its relatively high spin, this state, unlike the neighboring $1/2^-$ state, decays mainly to the 2^+ excited state in ^{6}He.

(v) An experimental controversy is related to the location of $1/2^-$ state in ^{7}He. In contrast to the findings of Refs. [47,48,56], the experimental study [57] finds this state to be lower in energy. Our calculation gives an excitation energy of 3.3 MeV for this resonance. However, the cross section obtained with the same Hamiltonian (Fig. 4) peaks at much lower energy and appears to be more consistent with [57]. The state is very broad; threshold effects and the presence of other states significantly influence the broad resonances, as we clearly record in our calculations. Because of this, a parametrization in terms of the width and resonance centroid may be quite ambiguous. This suggests a possible tentative explanation for the present uncertainty, although further studies are certainly needed.

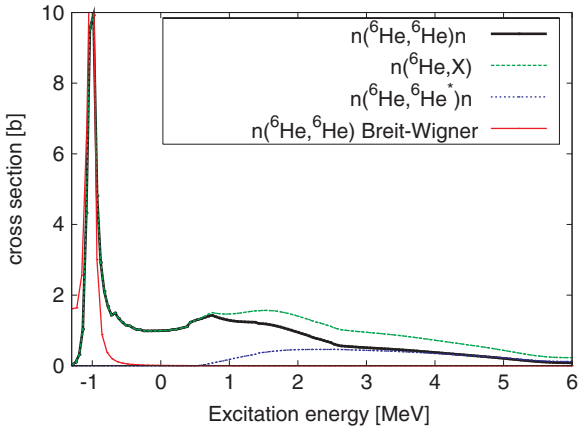

FIG. 4. (Color online) CSM results for ^{7}He isotopes. The full scattering cross section is plotted for several reactions: $n(^6\text{He}, ^6\text{He})n$—elastic neutron scattering off the ground state of ^{6}He; $n(^6\text{He}, X)$—total cross section of neutron scattering by ^{6}He; and $n(^6\text{He}, ^6\text{He}^*)n$—inelastic scattering of ^{6}He to the excited 2^+state. The remaining curve shows a typical Breit-Wigner shape for elastic scattering via the single $3/2^-$ resonance.

(vi) For the heaviest isotopes and, in particular, for the discussion of the presently interesting case of ^{9}He, the extension to the *sd* shell is necessary, especially in light of recent experimental evidence showing the ground state of ^{9}He to be $1/2^+$.

(vii) The scattering cross-section curves as a function of energy start from threshold and generally are not symmetric and have neither Gaussian nor Lorentzian shape. For low-lying states with the width big enough to reach threshold, the distortion is particularly noticeable.

(viii) For broad resonances, the identification of resonances (or poles of the scattering matrix) with a peak in the cross section is inadequate. Interference between different resonances, including rather remote ones, is significant in this case.

(ix) When it comes to reaction cross sections, the CSM method only extends the traditional techniques and does not invalidate old approaches for physically justified situations. As seen from Fig. 4, the narrow $J = 3/2^-$resonance is well described with a typical Breit-Wigner curve,

$$\sigma = \frac{\pi}{2k^2}\sum_{lj}\frac{(2J_r+1)}{(2J_i+1)}\frac{\Gamma_r^2}{(E-E_r)^2+\Gamma_r^2/4},$$

where $\Gamma_r = 91$ keV and $E_r = -1.016$ MeV are taken from the discrete calculation in Table I. The deviations at thresholds are known limitations of the Breit-Wigner approximation.

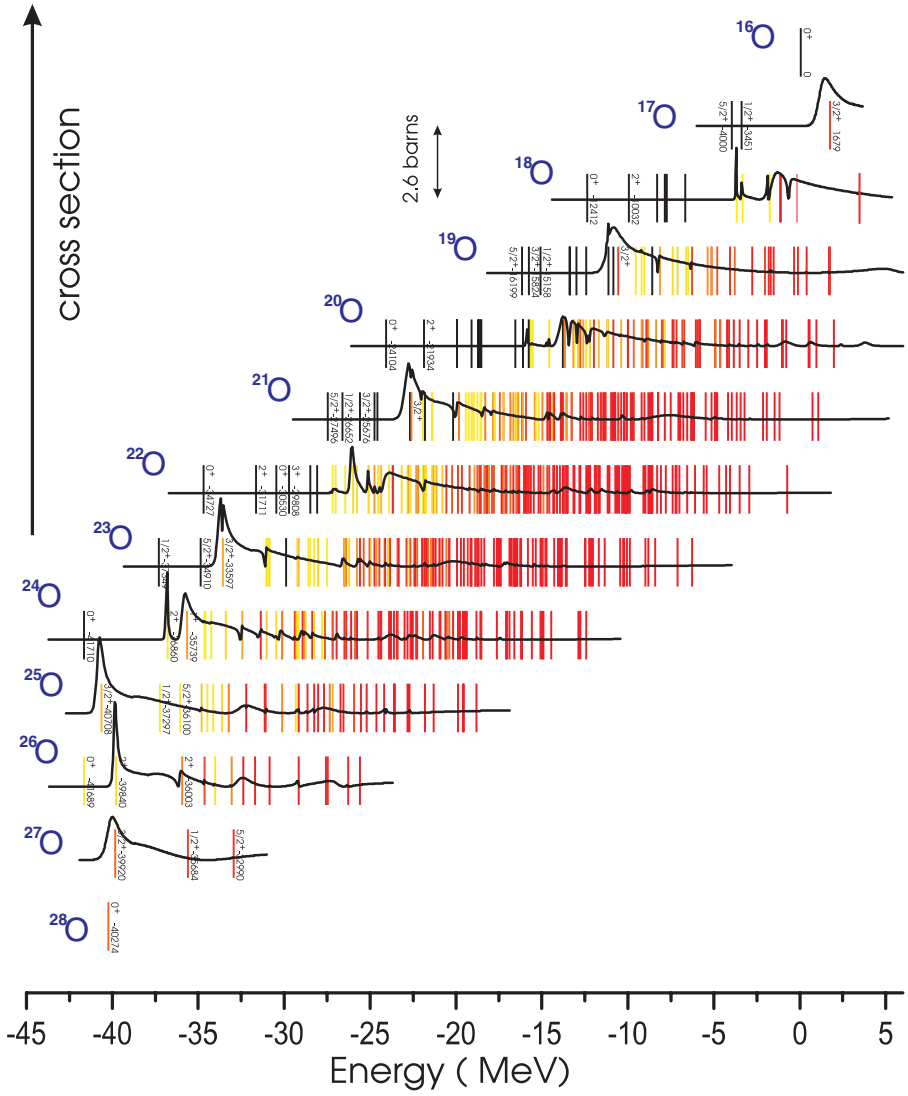

FIG. 5. (Color online) CSM calculation for oxygen isotopes with the HBUSD interaction. The states (vertical bars) are plotted as a function of energy relative to the ground state of ^{16}O. States shown with solid black lines are stable in our model; they are either below decay thresholds or with decays forbidden owing to the angular-momentum restrictions in the selected model space. States from yellow (color online)/lighter shade of gray (long lifetime) to red/darker gray (short lifetime) are resonance states. For some of the low-lying states the energy (in units of keV), spin and parity are given. Along with the resonance structure above thresholds, the elastic d-wave neutron scattering cross section, off the ground state of a daughter nucleus with $M = 0$ (even mass) or $M = 1/2$ (odd mass) magnetic quantum number, is plotted as a function of energy. The cross section is obtained as a part of the same CSM calculation.

C. Oxygen isotopes

The intrinsic space here is represented by the $s_{1/2}$, $d_{3/2}$, and $d_{5/2}$ s.p. orbitals composing the usual *sd* SM. The standard SM interactions (USD [30] or its slightly modified version for heavier isotopes, HBUSD [58]) were used in the calculations.

Since we use the Woods-Saxon potential for reaction calculations, it is important to make sure that the potential creates proper resonance states. For few low-lying s.p. resonances with large spectroscopic factors, we adjust the depth of the potential so that the correct s.p. resonance energy is indeed ensured. The Woods-Saxon potential parametrization with a mass-dependent depth [59,60] was demonstrated to reproduce the s.p. resonances and bound states with good precision for nuclei around mass $A = 16$. The parameters are the depth $V = 55.77$ MeV and the spin-orbit potential $V_{SO} = 25.6$ MeV; the radius $R = 3.05$ fm and diffuseness 0.65 fm are the same for the central and spin-orbit parts. For the majority of high-lying states, the potential was not readjusted and the decay amplitude was computed directly from Eq. (35). The resonance phenomenon in this case is due to the many-body effects, where the complexity of the many-body states makes the overlap in Eq. (52) small.

In Fig. 3 the widths of the resonant states $s_{1/2}$, $d_{3/2}$, and $d_{5/2}$ are shown as a function of their energy being found with the aid of the Woods-Saxon potential with variable depth. The curves are limited to the near-threshold region approximately determined as $kR < l$ (and $kR \ll 1$ for $l = 0$), where R is the nuclear radius. For oxygen, this limits the d wave at about 3 MeV. The curves are close to straight lines, displaying the appropriate power-law scaling (51) of the decay width as a function of energy. The lines can be fit by the equations (with ϵ in units of MeV) $\gamma(s_{1/2}) = 16\,\epsilon^{1/2}$, $\gamma(d_{3/2}) = 0.15\,\epsilon^{5/2}$, and $\gamma(d_{5/2}) = 0.04\epsilon^{5/2}$. These fits are shown with dashed lines.

In Fig. 5 we show an overview of the full CSM calculation for oxygen isotopes within the *sd* shell. Some of the first results were reported earlier [7,8].

Our calculations are in a good agreement with available experimental data for the oxygen isotopes [46,61]. One has to emphasize again that, with the assumption of the self-energy term Δ being a part of the conventional SM Hamiltonian, the

TABLE II. Lowest resonance states in the chain of oxygen isotopes. The experimental data on the left [EXP–energy of the state (in MeV), Q—energy above threshold (in MeV), and Γ—width (in keV)] are compared to the theoretical results on the right. The decay mode in the third column indicates the decay branches assumed by experimentalists [46,61].

A	j	Mode	EXP	Q	Γ	Theory	E	Q	Γ
17	$3/2^+$	γn	5.085	0.941	96	WS	4.5	1.0	122
18	2^+	$\gamma\alpha n$	8.213	0.169	1 ± 0.8	USD	9.465	1.242	200
18	1^+	αn	8.817	0.773	70 ± 12	USD	10.823	2.600	85
18	4^+	$\gamma\alpha n$	8.955	0.911	43 ± 3	USD	8.750	0.526	28
19	$5/2^+$	n	5.148	1.191	3.4 ± 1	USD	5.011	1.121	5.1
19	$9/2^+$		5.384	1.427	$\sim$0	USD	5.175	1.282	0
19	$3/2^+$	n	5.54	1.58	310	USD	5.529	1.636	290
19	$7/2^+$	n	6.466	2.509	small	USD	6.880	0.808[a]	63
24	2^+	n	?	?	?	HBUSD	4.850	0.489	18
26	0+	$2n$	0	?	?	HBUSD	0	0.021	0.02
28	0+	$2n$	0	?	?	HBUSD	0	0.345	14

[a]The Q value is measured for the excited state in the daughter system.

bound states are exactly the same as obtained in the usual SM calculation. The novelty appears when the states above decay thresholds are considered. The properties of a few experimentally identified resonances in oxygen isotopes are compared to the CSM predictions in Table II.

There are two cases in ^{17}O and ^{19}O corresponding to the neutron emission from the $d_{3/2}$ orbital. These rather pure s.p. decays do not involve much in the realm of many-body physics and so are well described with the Woods-Saxon potential model (Fig. 3). Here the SM may be used to predict the neutron decay energy; however, there is an obvious improvement if the experimental Q value is used in the s.p. reaction calculations. The power law for the energy dependence of the decay width can enhance the predictive power of the description.

The two-body case of ^{18}O is more complicated; however, there are only 14 states in the *sd* SM. The comparison of the level structure and neutron scattering cross section with data is shown in Fig. 6. The SM below the neutron decay threshold (zero on the plot) is in impressive agreement with the data. Here, for all *sd*-SM states shown with longer ticks (in red, color online), the experimental counterpart can be easily identified in the observed spectrum. Practically all remaining observed negative-parity states below neutron threshold can be identified with particle-hole excitations using the extended *p-sd-pf* SM. In the theoretical calculation, these states are shown with small lines (where the WBP cross-shell interaction from Ref. [31] was used).

Because of the resonant nature of states, the experimental picture above neutron decay threshold becomes more ambiguous. The lowest near-threshold state 2^+ may correspond to one of the higher lying 2^+ states in our model (see Fig. 6 and Table II). Because of the significant difference in energy above threshold between this state and its possible theoretical counterpart, comparison of the decay widths is inappropriate. Following this state, there are rather narrow 4^+ and 1^+ states (with the experimental assignment of 1^+ for the latter state still uncertain); see Table II and Fig. 6. Although in the theoretical calculation these states come out in a different order, their observed and calculated widths appear to agree. Beyond this point there are several broad, $\sim$(100–200) keV, unidentified resonances observed experimentally. They may be juxtaposed to the 150- to 400-keV wide 2^+, 3^+, and 1^+ states appearing in the CSM calculation. To support this argument, we show on the lower panel of Fig. 6 the CSM neutron scattering cross section computed using Eq. (15). Since this calculation takes into account only $l = 0$ and $l = 2$ partial waves, the peaks from negative-parity states do not appear. On the upper

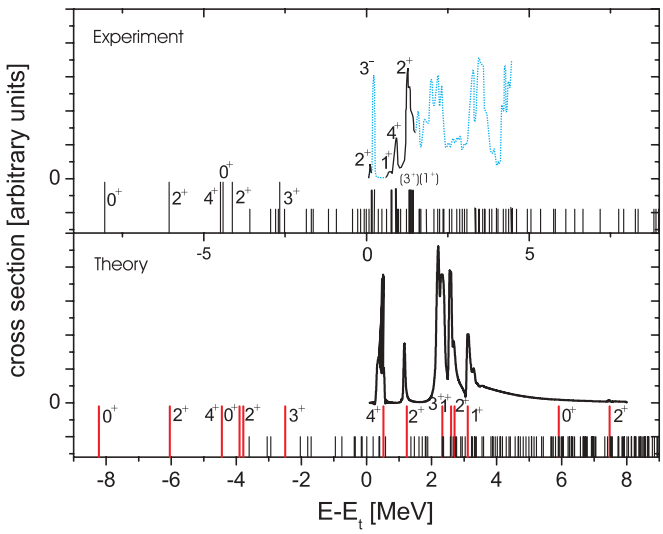

FIG. 6. (Color online) (Lower panel) The result of the CSM calculation of the level scheme and neutron scattering cross section from the ground state of ^{17}O. Marked levels corresponding to the *sd*-shell model states are included in the CSM calculation. All other levels result from the expanded *sd-pf* shell calculation (see text); the configurations of this type are not coupled to continuum and corresponding (negative-parity) states do not appear in the cross-section plot. (Upper panel) The empirical level scheme in ^{18}O. The neutron scattering cross section on the upper panel is indirectly inferred from the ^{14}C(αn)^{17}O reaction [62] and other compilations [61,63,64]. The parts of the cross section shown with a solid line are expected to be dominated by the positive-parity $l = 0$ or $l = 2$ partial waves and thus can be distantly juxtaposed to the curve on the lower plot.

plot we roughly reproduce the experimental cross section obtained from indirect reactions [61–64]. The portion of the curve corresponding to positive-parity resonances, which are expected to be present in the theoretical calculation, is shown by the solid black curve. There is a reasonable similarity in the resonant structure corresponding to the set of wide states 2^+, 3^+, and 1^+. In the experiment, the spin-parity assignments for the states shown in Fig. 6 in brackets have not yet been confirmed.

The cross-section picture indicates that our interpretation is plausible, although differences, by factors of 2 to 4, in the resonance parameters may be partly due to different definitions of the width used in the data analysis. The broadness of these resonances that causes difficulties in experimental analysis and interpretation of peaks is here a trivial consequence of the simple two-particle structure of ^{18}O, which implies high spectroscopic factors for s.p. decay. The situation changes for the next isotope, ^{19}O, where there is only one broad s.p. $3/2^+$ state that stands out in the calculations of the cross section. The majority of other states are narrow owing to the many-body complexity. They would not be visible on a plot of the cross section; however, this allows for the direct comparison of widths and energies shown in Table II.

Little is known about the heavier oxygen isotopes, although this situation will change in the near future as new radioactive beam experiments come online. In Table II we quote some (in our view) of the most interesting predictions of the model. The cases of ^{26}O and ^{28}O are just beyond the drip line. The ground states of these nuclei are unstable with respect to neutron pair emission. Section III D, although being centered around interactions, discussed how to tackle such cases. Unfortunately, the uncertainty in the effective interactions complicates the job of predicting. We have no firm knowledge about the interaction coupling internal states to the continuum and, unlike in the helium case, in the oxygen data we could not find a case to determine this coupling phenomenologically. Thus we only consider here the case of sequential decay driven by what we believe to be a well-defined one-body potential.

The second problem is that the traditional SM adjusted to experimental data near the stability line cannot be extrapolated with full certainty to the vicinity of drip lines. The role of the self-energy term $\Delta(E)$ is another question. Indeed, the well-established USD interaction predicts ^{26}O to be bound, which is known from experiments not to be the case. In our calculations we had to resort to the HBUSD interaction specifically adjusted to heavier isotopes. The Q value coming from this interaction in the case of ^{26}O is only 21 keV, whereas the typical SM uncertainty in level energies is about 200 keV. This uncertainty entering the power-law scaling of decay width versus energy makes the lifetime predictions unreliable.

Thus, collecting our calculations in Table II, we see our strongest prediction through Eq. (63). In both cases of ^{26}O and ^{28}O, the lowest $3/2^+, 1/2^+$, and $5/2^+$ states in the adjacent isotopes ^{25}O and ^{27}O are the main candidates for the intermediate states in the sequential two-body decay because of the low-energy barrier in combination with large spectroscopic factors of these mainly s.p. states. At the same time, in the case of ^{26}O we have neutron separation energies $S_{3/2} = 0.98$, $S_{1/2} = 4.39$, and $S_{5/2} = 5.54$ MeV; the corresponding spectroscopic factors are $\Upsilon_{3/2} = 0.28$, $\Upsilon_{1/2} = 0.019$, and $\Upsilon_{5/2} = 2.2 \times 10^{-4}$. In addition to spectroscopic information, the kinematics of the phase-space volume is another essential factor. A simple estimate with the aid of Eq. (63) shows that the transition through the s state would dominate throughout the entire region below s.p. threshold. Owing to level energetics, two-body decay remains significant even in the presence of the open one-body channel. However, the simple power-law scaling used to obtain the phase-space integrals of Eq. (62) may no longer be valid high above threshold. If the ground state in ^{26}O were at $E_t = 1$ MeV above the two-neutron decay threshold, while still right at the opening of the one-neutron decay channel into the $3/2^+$ state of ^{25}O, $S_{3/2} = 0$, the decay width coming from sequential decay would be about 30 keV, as opposed to the value of 20 eV in Table II quoted for $E_t = 0.021$ MeV.

V. CONCLUSION

The first goal of this work is to present a systematic and detailed discussion of the continuum shell model as a step toward unifying the nuclear structure with nuclear reactions. We amplify and extend the ideas and methods started in our earlier works [7,8]. In this presentation we clarify the CSM formalism and show its relation to the standard SM. One of the important points of this work is the physical interpretation of various results. On the shell model side, we highlight the meaning of solutions of the energy-dependent non-Hermitian effective Hamiltonian and identify the procedures to be taken in relation to different definitions of resonance states. On the reaction side, we show how the scattering matrix, cross sections, and related quantities can be calculated; the unitarity properties of the scattering matrix built in the model are emphasized.

The general discussion of s.p. decays centers around the potential s.p. problem. Not only is this textbook problem a central part of the calculations, but it also provides an important parallel to the full CSM description. In the case of a particle in a potential well, the Gamow states, decay amplitudes, and scattering matrix can be calculated through numerical solutions of the s.p. Schrödinger equation in coordinate space. This allows one to establish a transparent relation and interpretation of the same quantities in the full CSM.

The consideration of two-body decays is one of the significant advances of the present formulation. Considering the one- and two-body terms in the part of the Hamiltonian that links the internal shell model and external reaction space we get keys to the sequential and direct decays, respectively. In the case of sequential decay, a second-order one-body process, we discuss the transition through the resonance tail, namely the role of broad one-body resonances located in the intermediate nucleus above threshold. The direct, or correlated, decay processes are strongly related to the problem of pairing and other coherent effects in the continuum, especially in the case of neutron excess. This problem, important also for the physics of neutron stars, is still far from being solved.

The last section of this work shows practical applications of the model. The self-consistency in energy, proper open channels and realistic reaction calculations, and parent-daughter structure relations through the decay chain are discussed as the essential elements of the model. The diagonalization of the full Hamiltonian with both Hermitian and non-Hermitian parts is emphasized as an important component for treating properly the mutual influence of structure and reactions. Discussion of the extreme effects of this nature, such as super-radiance, lies outside the scope of this paper (see Refs. [25,49,50]).

Another goal of this work is to report the advance in practical applications of the CSM and in particular to demonstrate new cross-section calculations performed in the same unified framework and presented along with the bound states and resonance parametrizations. Comparison with experimental data indicates a satisfactory agreement for both helium and oxygen isotopes. The possible role of sequential decay in heavy oxygen isotopes is discussed and predictions for the decay width are given. Upcoming experimental data will be instrumental for further development of the theory.

We mentioned but did not discuss here the computational problems, which are of a higher level of difficulty compared to those for the normal SM. In fact, the novel methods for constructing Green's functions for large-scale calculations using the Chebyshev polynomial expansion and Woodbury equation stand behind the presented results. Technical and numerical details, with possible applications to other problems, will be presented elsewhere. From the conceptual viewpoint, the basic question of effective interactions remains unsolved. We used here a semiempirical method of combining the SM experience with finding the missing cross-space matrix elements from the solution of the scattering problem and numerical fits based on general requirements of quantum-mechanical threshold behavior. The inclusion of giant resonances, more complicated decay modes, and cluster channels is also on the agenda for future work.

ACKNOWLEDGMENTS

The authors acknowledge support from the U. S. Department of Energy, Grant No. DE-FG02-92ER40750, Florida State University FYAP award for 2004, and the National Science Foundation, Grant Nos. PHY-0070911 and PHY-0244453. Help from and useful discussions with B.A. Brown and G. Rogachev are highly appreciated.

[1] V. Zelevinsky, ed., *Nuclei and Mesoscopic Physics*, edited by V. Zelevinsky, AIP Conf. Proc. No. 777 (AIP, New York, 2005).
[2] B. A. Brown, Prog. Part. Nucl. Phys. **47**, 517 (2001).
[3] J. Fridmann *et al*., Nature **7044**, 922 (2005).
[4] P. Hansen and B. Sherrill, Nucl. Phys. **A693**, 133 (2001).
[5] E. Caurier, G. Martinez-Pinedo, F. Nowacki, A. Poves, and A. P. Zuker, Rev. Mod. Phys. **77**, 427 (2005).
[6] C. Mahaux and H. Weidenmüller, *Shell-Model Approach to Nuclear Reactions* (North-Holland, Amsterdam, 1969).
[7] A. Volya and V. Zelevinsky, Phys. Rev. C **67**, 54322 (2003).
[8] A. Volya and V. Zelevinsky, Phys. Rev. Lett. **94**, 052501 (2005).
[9] H. Feshbach, Ann. Phys. (NY) **5**, 357 (1958).
[10] H. Feshbach, Ann. Phys. (NY) **19**, 287 (1962).
[11] I. Rotter, Rep. Prog. Phys. **54**, 635 (1991).
[12] I. Rotter, Phys. Rev. E **64**, 036213 (2001).
[13] V. Weisskopf and E. Wigner, Z. Phys. **63**, 54 (1930).
[14] O. Rice, J. Chem. Phys. **1**, 375 (1933).
[15] U. Fano, Nuovo Cim. **12**, 156 (1935).
[16] U. Fano, Phys. Rev. **124**, 1866 (1961).
[17] R. Id Betan, R. J. Liotta, N. Sandulescu, and T. Vertse, Phys. Rev. Lett. **89**, 042501 (2002).
[18] N. Michel, W. Nazarewicz, M. Ploszajczak, and K. Bennaceur, Phys. Rev. Lett. **89**, 042502 (2002).
[19] N. Michel, W. Nazarewicz, M. Ploszajczak, and J. Okolowicz, Phys. Rev. C **67**, 054311 (2003).
[20] N. Michel, W. Nazarewicz, and M. Ploszajczak, Phys. Rev. C **70**, 064313 (2004).
[21] J. Okolowicz, M. Ploszajczak, and I. Rotter, Phys. Rep. **374**, 271 (2003).
[22] G. Hagen, M. Hjorth-Jensen, and J. S. Vaagen, Phys. Rev. C **71**, 044314 (2005).
[23] C. A. Engelbrecht and H. A. Weidenmüller, Phys. Rev. C **8**, 859 (1973).
[24] L. Durand, Phys. Rev. D **14**, 3174 (1976).
[25] V. Sokolov and V. Zelevinsky, Nucl. Phys. **A504**, 562 (1989).
[26] T. Berggren, Nucl. Phys. **A109**, 265 (1968).
[27] A. F. J. Siegert, Phys. Rev. **56**, 750 (1939).
[28] G. Breit and E. Wigner, Phys. Rev. **49**, 519 (1936).
[29] A. Holt, T. Engeland, M. Hjorth-Jensen, and E. Osnes, Nucl. Phys. **A634**, 41 (1998).
[30] B. A. Brown and B. Wildenthal, Annu. Rev. Nucl. Part. Sci. **38**, 29 (1988).
[31] B. A. Brown, A. Etchegoyen, and W. Rae, Technical Report No. MSU-NSCL 524, NSCL, Michigan State University, 1994 (unpublished).
[32] A. Bohr and B. Motttelson, *Nuclear Structure*, vol. I (World Scientific, Singapore, 1998).
[33] L. Landau and E. Lifshitz, *Quantum Mechanics, Non-relativistic Theory,* 3rd ed. (Pergamon Press, New York, 1981).
[34] E. Merzbacher, *Quantum Mechanics* (Wiley, New York, 1998).
[35] C. N. Davids and H. Esbensen, Phys. Rev. C **61**, 054302 (2000).
[36] V. Burgov and S. Kadmensky, Sov. J. Nucl. Phys. **49**, 967 (1989).
[37] V. Burgov and S. Kadmensky, Phys. At. Nucl. **59**, 424 (1996).
[38] A. Baz, I. Zeldovich, and A. Perelomov, *Scattering, Reactions and Decay in Nonrelativistic Quantum Mechanics* (Israel Program for Scientific Translations, Jerusalem, 1969).
[39] E. Wigner, Phys. Rev. **73**, 1002 (1948).
[40] V. Zelevinsky and A. Volya, in *Challenges of Nuclear Structure*, ed. A. Covello (World Scientific, Singapore, 2002), p. 261.
[41] R. Dicke, Phys. Rev. **93**, 99 (1954).
[42] J. Rotureau, J. Okolowicz, and M. Ploszajczak, Phys. Rev. Lett. **95**, 042503 (2005).
[43] B. A. Brown and F. C. Barker, Phys. Rev. C **67**, 041304(R) (2003).
[44] L. V. Grigorenko and M. V. Zhukov, Phys. Rev. C **68**, 054005 (2003).
[45] F. C. Barker, Phys. Rev. C **59**, 535 (1999).
[46] Evaluated nuclear structure data file, http://www.nndc.bnl.gov.

[47] G. V. Rogachev *et al*., Phys. Rev. Lett. **92**, 232502 (2004).
[48] A. A. Korsheninnikov *et al*., Phys. Rev. Lett. **82**, 3581 (1999).
[49] N. Auerbach, V. Zelevinsky, and A. Volya, Phys. Lett. **B590**, 45 (2004).
[50] A. Volya and V. Zelevinsky, J. Opt. B **5**, S450 (2003).
[51] T. Teichmann, Phys. Rev. **77**, 506 (1950).
[52] T. Teichmann and E. Wigner, Phys. Rev. **87**, 123 (1952).
[53] S. Cohen and D. Kurath, Nucl. Phys. **A73**, 1 (1965).
[54] J. Stevenson *et al*., Phys. Rev. C **37**, 2220 (1988).
[55] J. L. Wiza and R. Middleton, Phys. Rev. **143**, 676 (1965).
[56] A. H. Wuosmaa *et al*., Phys. Rev. C **72**, 061301(R) (2005).
[57] M. Meister *et al*., Phys. Rev. Lett. **88**, 102501 (2002).
[58] B. A. Brown, W. Richter, R. Julies, and B. Wildenthal, Ann. Phys. (NY) **182**, 191 (1988).
[59] B. Skorodumov *et al*., Phys. At. Nucl., in press; nucl-ex/0609040.
[60] V. Goldberg *et al*., Phys. Rev. C **69**, 031302(R) (2004).
[61] D. Tilley, C. Cheves, J. Kelley, S. Raman, H. Weller, and F. Ajzenberg-Selove, Energy Levels of Light Nuclei, $A = 3$–20, http://www.tunl.duke.edu/nucldata.
[62] J. K. Bair, J. L. C. Ford Jr., and C. M. Jones, Phys. Rev. **144**, 799 (1966).
[63] S. F. Mughabghab, R. Kinsey, and C. Dunford, *Neutron Cross Sections Series* (Academic Press, New York, 1981).
[64] V. McLane, C. Dunford, and P. Rose, *Neutron Cross Section Curves*, Vol. 2 (Academic Press, Boston, 1988).